High-resolution absorption spectroscopy of the deep impurities S and Se in ^{28}Si revealing the ^{77}Se hyperfine splitting

M. Steger, A. Yang, and M. L. W. Thewalt*
Department of Physics, Simon Fraser University, Burnaby, British Columbia, Canada V5A 1S6

M. Cardona
Max-Planck-Institut für Festkörperforschung, 70569 Stuttgart, Germany

H. Riemann and N. V. Abrosimov
Institute for Crystal Growth (IKZ), 12489 Berlin, Germany

M. F. Churbanov, A. V. Gusev, A. D. Bulanov, and I. D. Kovalev
IChHPS of the RAS, 603000 Nizhny Novgorod, Russia

A. K. Kaliteevskii and O. N. Godisov
Science and Technical Center "Centrotech," 198096 St. Petersburg, Russia

P. Becker
Physikalisch-Technische Bundestanstalt Braunschweig, 38116 Braunschweig, Germany

H.-J. Pohl
VITCON Projectconsult GmbH, 07743 Jena, Germany

E. E. Haller and J. W. Ager III
University of California Berkeley and LBNL, Berkeley, California 94720, USA
(Received 2 July 2009; published 10 September 2009)

Recently, studies have demonstrated remarkable improvements in absorption spectroscopy of shallow impurities by using highly enriched ^{28}Si to eliminate the inhomogeneous isotope broadening inherent in natural Si. Here, we show that similar dramatic improvements in the linewidths of electronic transitions can be achieved with the two chalcogens sulfur and selenium in ^{28}Si. The S^+ and Se^+ $1s(T_2)$ transitions exhibit a full width at half maximum of only 0.008 cm^{-1} for the Γ_7 component—more than one order of magnitude sharper than in natural silicon and a factor of 1.5 narrower than the width of the sharpest shallow impurity transition in ^{28}Si. Hence they are the narrowest lines ever seen for impurity states in silicon. Fine structure is revealed in the absorption spectrum of the Se double donor and the $^{77}Se^+$ $1s(T_2)$ Γ_7 transition shows a splitting due to a hyperfine coupling with the $I=1/2$ nuclear spin. Under an applied magnetic field, the electronic, and nuclear spins can be individually determined with potential applications in quantum computing.

DOI: 10.1103/PhysRevB.80.115204 PACS number(s): 78.30.Am, 71.55.Cn

I. INTRODUCTION

It has been shown[1–4] that the isotopic randomness present in ^{nat}Si produces a significant inhomogeneous broadening of many of the ground state to excited-state infrared absorption transitions of the shallow donor phosphorus (P) and the acceptor boron (B). Thus, many of these transitions are much sharper in isotopically enriched ^{28}Si than in natural Si (^{nat}Si). It was also found that the impurity binding energy depends on both the host isotope mass[2] and the isotopic composition of the impurity itself.[1] Due to the significantly narrower linewidths of the absorption lines in ^{28}Si, this can lead to an apparent splitting of the absorption lines when different impurity isotopes are present.

While the earlier work with ^{28}Si has been done on shallow impurities,[1–4] the focus in this work lies on the deep double donors S and Se, for which we have recently presented preliminary results.[5,6] By using isotopically enriched ^{28}Si and ^{30}Si together with a number of different isotopic compositions of sulfur (S) and selenium (Se), we observe similar effects as for B and P. We see a reduction of the full width at half maximum (FWHM) of many (but not all) absorption lines. The random placement of different Si isotopes in the close vicinity of the impurity center causes satellite peaks for the S^+ $1s(T_2)$ transition.[7] These satellites are removed in highly enriched ^{28}Si. We show that these satellite peaks can also be seen for $^{77}Se^+$ in ^{nat}Si. Due to the sharpness of the absorption lines in ^{28}Si we are able to resolve the hyperfine splitting of the $^{77}Se^+$ ground state and to optically determine both electronic and nuclear spins. Furthermore, we report on energy shifts depending on the isotopic mass of the dopants S and Se and the Si host material.

II. THEORY

The chalcogens S and Se give rise to a number of different donor centers in Si.[8] These centers can involve one, two

or more sulfur or selenium atoms and can be either neutral or ionized. In this work we investigated the centers S^0, S^+, S_2^0, Se^0, and Se^+. Here the superscript of the label denotes the ionization state of the donor, while the subscript indicates the number of atoms comprising the impurity center with "2" standing for an impurity pair.

The S^0, S^+, Se^0, and Se^+ impurity centers are substitutional and occupy a tetrahedral site in the silicon host lattice. The electronic structure of these centers is heliumlike, which is to say that isolated substitutional chalcogen impurities in Si are double donors. The p state spectra are quite "hydrogenic" and comparable to phosphorus p states,[8,9] except of course the p state binding energies for the singly ionized centers are four times those of the neutral centers.

Due to their deep nature, the s states, and particularly $1s$, can have transitions which are not observed for shallow donors. For donor atoms occupying tetrahedral lattice sites the central cell potential splits the sixfold degenerate s state into a singlet (A_1), a triplet (T_2), and a doublet (E).[8,10] This valley-orbit splitting is strongest for the $1s$ state. Including spin, the symmetry representations A_1, E, and T_2 become Γ_6, Γ_8, and $\Gamma_7+\Gamma_8$, respectively. The transitions $1s(A_1) \rightarrow 1s(T_2)$ and $1s(A_1) \rightarrow 1s(E)$ are effective mass theory (EMT) forbidden but the T_2 transition is symmetry allowed.[10,11] The fact that the T_2 transition is only partially allowed contributes to its long lifetime and therefore to a narrow linewidth making it possible to resolve the ^{77}Se hyperfine splitting using this final state.

The inhomogeneous broadening of the impurity absorption transitions in ^{nat}Si have been explained as a result of the isotopic randomness present in the silicon host material.[1–3] The broadening seen in ^{nat}Si, or any sample of mixed isotopic composition, is dominated by an effect which is independent of the small shifts in binding energy between pure ^{28}Si, ^{29}Si, and ^{30}Si. The ground state wave functions of the impurities are compact, and sample a relatively small volume surrounding the impurity ion. Hence in natural Si these wave functions are subject to relatively large fluctuations of the actual isotopic composition within this effective volume. These fluctuations in turn induce shifts of the ground-state energies, which can be related to the known shifts of the conduction band energies with average isotopic composition. The excited state wave functions, on the other hand, are much more extended, and therefore sample isotopic compositions much closer to the average composition than the ground-state wave function does. The different isotopic composition sampled by individual ground states leads to an inhomogeneous broadening which is expected to become larger for deeper and thus more compact ground states.

By using highly enriched ^{28}Si this random distribution of isotopes can be eliminated and the inhomogeneous broadening removed. We are then often left with homogeneous broadening due to the lifetime of the excited state, as indicated by a Lorentzian line shape.

III. EXPERIMENTAL METHOD

Our ^{28}Si material was used before for photoluminescence (excitation) experiments.[12–14] It has an isotopic composition of 99.991% ^{28}Si+0.0075% ^{29}Si+0.0015% ^{30}Si. While the chemical purity of the ^{28}Si sample is improved as compared to previous material,[1,2] it does not match that of ultrahigh purity (UHP) natural Si. The ^{30}Si sample contains 2.50% ^{28}Si+7.70% ^{29}Si+89.80% ^{30}Si.[15] Natural silicon has isotope abundances of 92.22% ^{28}Si+4.69% ^{29}Si+3.09% ^{30}Si. The dopants were of high chemical purity. Natural sulfur has 94.93% ^{32}S and 4.29% ^{34}S, with other isotopes at less than 1%. The ^{34}S and ^{77}Se materials were isotopically enriched to >90% and 97.1%, respectively. A combination of samples with different host materials and different isotopes of the dopants S and Se were prepared as described in literature.[8,10,16] A Bomem DA8 Fourier transform spectrometer was used to obtain the infrared absorption spectra with instrumental resolutions of up to 0.003 cm^{-1}. The actual resolution was verified to be better than 0.007 cm^{-1} with the help of gas lines. The spectrometer's internal light sources were used together with appropriate beam splitters (Globar with KBr beam splitter and quartz halogen lamp with CaF_2). Liquid nitrogen cooled HgCdTe, InSb, and InAs detectors were used according to the desired energy range. The samples were loosely held in place on the sample holder, with their own weight being the only force on them, to avoid any mechanical strain and immersed in superfluid helium at a temperature of 1.5 K.

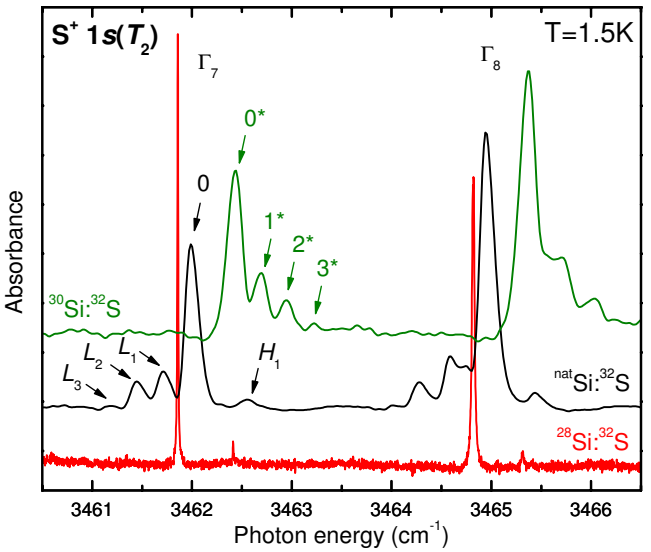

FIG. 1. (Color online) Energy shifts of S^+ $1s(T_2)$ with different Si host isotope compositions. Due to the stronger sharpening of the $1s(T_2)$ Γ_7 transition, the Γ_7/Γ_8 intensity ratio is reversed in ^{28}Si. L_1, L_2, and L_3 are a Si nearest-neighbor-isotope effect. Remnants of ^{34}S are visible in the ^{28}Si spectrum (H_1). Spectra recorded at 1.5 K with a resolution of 0.004 cm^{-1} (^{28}Si), 0.050 cm^{-1} (^{30}Si), and 0.100 cm^{-1} (^{nat}Si).

IV. RESULTS AND DISCUSSION

A. S^+ and Se^+ centers

The S^+ $1s(T_2)$ spectra of ^{32}S in ^{28}Si, ^{nat}Si, and ^{30}Si is shown in Fig. 1. The two absorption lines originate from the $1s(A_1) \rightarrow 1s(T_2)$ transition. The final state is split into Γ_7 and

TABLE I. Energies and FWHM of S^+ $1s(T_2)$ Γ_7 and Γ_8 for different host and impurity isotope combinations. All energies in cm^{-1}.

Γ_7	E	FWHM
$^{28}Si:^{32}S$ "0"	3461.858	0.010
$^{28}Si:^{34}S$ "0"	3462.409	0.008
$^{nat}Si:^{32}S$ "0"	3461.986	0.16
$^{nat}Si:^{32}S$ L_1	3461.709	0.13
$^{nat}Si:^{32}S$ L_2	3461.445	0.16
$^{nat}Si:^{32}S$ L_3	3461.184	
$^{nat}Si:^{34}S$ H_1	3462.555	0.20
$^{30}Si:^{32}S$ "0*"	3462.430	0.17
$^{30}Si:^{32}S$ "1*"	3462.696	0.13
$^{30}Si:^{32}S$ "2*"	3462.952	0.20
$^{30}Si:^{32}S$ "3*"	3463.208	0.15
Γ_8		
$^{28}Si:^{32}S$ "0"	3464.819	0.030
$^{28}Si:^{34}S$ "0"	3465.308	0.022
$^{nat}Si:^{32}S$ "0"	3464.948	0.17
$^{nat}Si:^{32}S$ L_1	3464.590	0.18
$^{nat}Si:^{32}S$ L_2	3464.275	0.16
$^{nat}Si:^{32}S$ L_3	3464.014	
$^{nat}Si:^{34}S$ H_1	3465.457	0.21
$^{30}Si:^{32}S$ "0*"	3465.373	0.19
$^{30}Si:^{32}S$ "1*"	3465.713	0.22
$^{30}Si:^{32}S$ "2*"	3466.007	0.21

Γ_8 representations (see Table I for transition energies). Low energy satellites L_1, L_2, and L_3 can be seen for the Γ_7 and Γ_8 transition in ^{nat}Si. These satellites are due to local vibrational modes (LVM) and are a Si nearest-neighbor isotope effect.[7] The "0" transition is due to a center having four ^{28}Si nearest neighbors, while L_1 has one ^{28}Si replaced with a ^{29}Si. L_2 results from either one ^{28}Si replaced with a ^{30}Si or two ^{28}Si atoms replaced with two ^{29}Si. A $^{29}Si^{30}Si$ replacement is responsible for L_3. In addition to this, the figure also shows high-energy satellites H_1, originating from a S isotope effect (^{34}S) which we will discuss later. When the probabilities (normalized to line "0") for L_1, L_2, and L_3 are calculated using the natural abundances of Si isotopes, one finds 0.20, (0.13+0.02), and 0.02, respectively. This agrees very well to our measured normalized intensities (to "0") of (0.21 ± 0.01) and (0.15 ± 0.04), L_3 is too weak for a useful comparison.

The isotopic enrichment of our ^{30}Si sample is similar to the one of natural Si with the difference that here ^{30}Si is enriched to approximately 89.80% and it contains roughly as much ^{29}Si and ^{28}Si as ^{nat}Si contains ^{29}Si and ^{30}Si. In Fig. 1 it is immediately visible that the order of the L_n satellite peaks is reversed in ^{30}Si, thus confirming that they are a Si nearest-neighbor isotope effect which is reversed here due to the opposite sign of the mass differences. Using the known enrichment, the normalized calculated intensities for "1*," "2*," and "3*" are 0.34, 0.15, and 0.03, respectively. This compares reasonably well to the normalized measured values of 0.36, 0.19, and 0.05 (all ± 0.01), given that the sample has a gradient in the enrichment.[15]

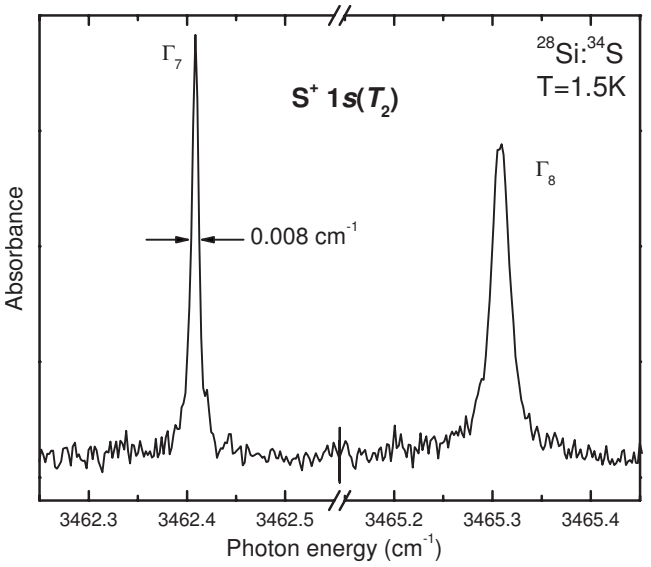

FIG. 2. Detailed fine structure of $^{34}S^+$ $1s(T_2)$ absorption lines in ^{28}Si with a resolution of 0.0024 cm^{-1} at a temperature of 1.5 K. The FWHM of the $1s(T_2)$ Γ_7 absorption line is only 0.008 cm^{-1} and 0.022 cm^{-1} for the $1s(T_2)$ Γ_8 line.

Figure 1 also shows the $1s(T_2)$ spectrum of $^{28}Si:^{32}S$, while a more detailed spectrum of $^{28}Si:^{34}S$ can be seen in Fig. 2 (see Table I for energies). The direct comparison in the first figure impressively exhibits the isotope broadening effect. In ^{28}Si we see a dramatic sharpening of both transitions, especially for the lower-energy Γ_7 state. In addition, the L_n satellite peaks are removed due to the absence of ^{29}Si or ^{30}Si and H_1, the transition due to ^{34}S is clearly resolved.

Figure 3 compares the Se^+ $1s(T_2)$ Γ_7 transition for several combinations of Se and Si isotopic compositions. By using ^{77}Se in ^{nat}Si this structure is simplified significantly. The spectrum then closely resembles the one of sulfur showing the same Si nearest-neighbor-isotope effects on the low-energy side. Table II lists the energies for this transition in different samples/isotopic compositions. For $^{nat}Si:^{nat}Se$ a broad peak showing some partially resolved structure and a long low-energy tail is observed.[7]

As the inhomogeneous Si isotope broadening is removed in ^{28}Si, well separated contributions of all stable Se isotopes are revealed as sharp lines with intensities corresponding well to the isotope abundance in ^{nat}Se. The Se isotope shift per amu for Se^+ $1s(T_2)$ Γ_7 is found to be -0.0737 cm^{-1} (-9.1 μeV), with the heavier isotope being at higher energy. This is in reasonable agreement with the value of -11 μeV estimated from a fitting of the $^{nat}Si:^{nat}Se$ spectrum.[7] All even numbered Se isotopes have single lines in the spectrum, only ^{77}Se is split into two lines and thus does not lie mid way between ^{76}Se and ^{78}Se. Unlike the other isotopes, ^{77}Se has a nuclear spin of $I=1/2$, causing a hyperfine splitting of the $^{77}Se^+$ ground state (see below). The energies of the Se^+ $1s(T_2)$ transition are given in Table II for different Se isotopes together with their FWHM.

As for sulfur, the sharpest absorption transition in the selenium spectrum in ^{28}Si is the Se^+ $1s(T_2)$ Γ_7 transitions. Fig-

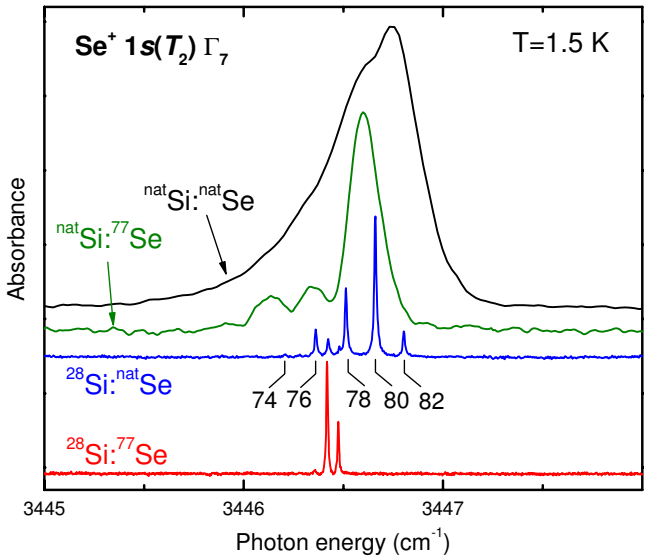

FIG. 3. (Color online) Absorption spectra of the Se^+ $1s(T_2)$ Γ_7 transition for several combinations of impurity and host isotopic composition. The $^{nat}Si:^{nat}Se$ spectrum at the top was obtained from Fig. 4 of Pajot *et al.* (Ref. 7) Transitions due to the stable isotopes of Se are resolved in the $^{28}Si:^{nat}Se$ spectrum, and are indicated by labels. The ^{77}Se hyperfine doublet dominates the spectrum of the $^{28}Si:^{77}Se$ sample at the bottom.

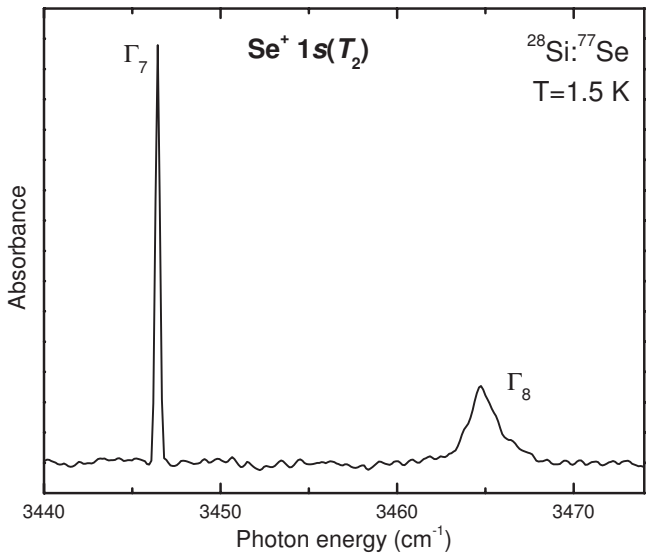

FIG. 4. Low-resolution spectrum of Se^+ $1s(T_2)$ in ^{28}Si. Spectrum recorded at a temperature of 1.5 K with a resolution of 0.25 cm^{-1}.

ure 4 shows the Γ_7 and Γ_8 components at low resolution. While the Γ_8 absorption line is inherently broad, the Γ_7 component sharpens dramatically. In the high-resolution spectrum of S^+ $1s(T_2)$ of ^{34}S in ^{28}Si shown in Fig. 2 we measure a FWHM of only 0.008 cm^{-1} for the $1s(T_2)$ Γ_7 line and 0.022 cm^{-1} for the Γ_8 absorption line. Similarly for Se, where the $^{77}Se^+$ $1s(T_2)$ Γ_7 singlet hyperfine component has a FWHM of only 0.008 cm^{-1} (Fig. 6). This makes the two Γ_7 transitions the narrowest donor or acceptor absorption lines observed in Si to date—they are ~22 times narrower than in previous S spectra[7] and narrower than P and B absorption transition lines in ^{28}Si by a factor of 1.5.[4] This exceptional result can be explained by the fact that the $1s(A_1) \rightarrow 1s(T_2)$ transition is forbidden in EMT but symmetry allowed and thus has an unusually long radiative lifetime. At 1.5 K curve fitting indicates that the S^+ and Se^+ (singlet) Γ_7 transitions have a 100% Lorentzian shape, showing that they are lifetime limited, while S^+ Γ_8 is only 88% Lorentzian. In an experiment at 4.2 K the FWHM of S^+ Γ_7 increased by 60% but kept its Lorentzian shape, while S^+ Γ_8 increased by only 20%. At elevated temperatures thermally activated transitions reduce the lifetime of the Γ_7 final state and thus increase the linewidth.

TABLE II. Energies and FWHM of Se^+ $1s(T_2)$ Γ_7 and Γ_8 for different host and impurity isotope combinations ‡ is from a low resolution spectrum, all energies in cm^{-1}.

Γ_7	E	FWHM
$^{nat}Si:^{nat}Se$ "0"	3446.742	0.5
$^{nat}Si:^{77}Se$ "0"	3446.609	0.18
$^{nat}Si:^{77}Se$ L_1	3446.346	0.11
$^{nat}Si:^{77}Se$ L_2	3446.141	0.18
$^{28}Si:^{74}Se$ "0"	3446.207	
$^{28}Si:^{76}Se$ "0"	3446.362	0.012
$^{28}Si:^{77}Se$ "0" triplet	3446.419	0.010
$^{28}Si:^{77}Se$ "0" singlet	3446.475	0.008
$^{28}Si:^{78}Se$ "0"	3446.513	0.013
$^{28}Si:^{80}Se$ "0"	3446.661	0.013
$^{28}Si:^{82}Se$ "0"	3446.804	0.013
Γ_8		
$^{nat}Si:^{nat}Se$ "0"	3464.88	1.9
‡$^{28}Si:^{77}Se$ "0"	3464.74	1.9

In the overlay shown in Fig. 1 it is clearly visible that a change in the host isotope composition not only gives rise to the satellites discussed earlier, but also introduces a shift of the binding energy. Both the band-gap energy and the impurity binding energy E_B increase with increasing host isotopic mass[2] and therefore we see the absorption transition of S in ^{30}Si above the one in ^{nat}Si and ^{28}Si. If one would determine the Si isotope shift between ^{28}Si and ^{30}Si it has to be taken into account that we observe two overlaying effects here. On the one hand a strictly electronic shift due to the average mass of the crystal,[2] on the other hand a shift due to nearest-neighbor LVM. To separate out these two shifts one would need to compare absorption lines of centers with the same surrounding cluster (such as $^{28}Si_4$) in the two different substrate materials.

The impurity isotope shift has been discussed before,[17,18] in particular for B in Si.[1,4] In the case of the acceptor B in Si the heavier isotope ^{11}B has a lower binding energy than the lighter ^{10}B, thus we see the absorption lines of ^{11}B at a lower energy than those of ^{10}B, which is the normal sign for impurity isotope shifts. However, for the S^+ $1s(T_2)$ transitions we observe that the ^{32}S-associated absorption lines are at lower energy than the ones of ^{34}S (H_1), so that $E(^{32}S) - E(^{34}S) =$

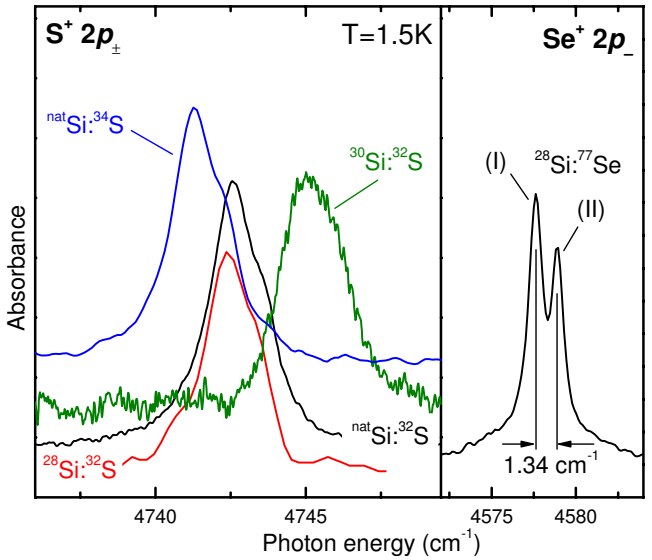

FIG. 5. (Color online) S^+ $2p_\pm$ in four different samples showing host (Si) and impurity (S) isotope shifts. The ^{nat}Si and ^{28}Si samples all show a higher-energy shoulder. $^{77}Se^+$ $2p_\pm$ is shown on the right side. It is clearly visible that in an otherwise perfect sample the $2p_\pm$ transition is split by 1.34 cm^{-1}. All spectra were recorded at a temperature of 1.5 K with a resolution of 0.500 cm^{-1} or better.

-0.56 cm^{-1} for Γ_7 and -0.50 cm^{-1} for Γ_8 (that is -0.28 cm^{-1} or -34.7 μeV and -0.25 cm^{-1} or -31.0 μeV per amu, respectively). Similarly for Se^+ $1s(T_2)$, the absorption lines due to the lighter Se isotopes are at lower energy. For shallow impurities, only the ground state undergoes a significant impurity mass dependent isotope shift, while the excited states all remain at the same energy. The S p transitions and S^0 and Se^0 $1s(T_2)$ show the same sign of the shift as shallow impurities do. In contrast, the S^+ and Se^+ $1s(T_2)$ state is rather deep. This, together with a $T_2 \otimes \tau_2$ vibronic coupling, can lead to a reversed isotope shift of the $1s(T_2)$ transition, as suggested by Pajot *et al.*[7]

We did not work extensively toward improving the S^+ p-state spectrum since the main attention was focused on the much sharper $1s(T_2)$ transition. Besides the $2p_\pm$ absorption only the ^{nat}Si:^{nat}S sample shows some of the weaker features. Those are the S^+ transitions $2p_0$(4581.52 cm^{-1}), $2s(T_0)$ (4622.23 cm^{-1}), $3p_0$, $4p_0$, $3p_\pm$, $4p_\pm$, and $5p_\pm$. In all samples the absorption lines have a Lorentzian shape, indicating that their FWHM is lifetime limited. In fact no significant difference in the FWHM in between the ^{28}Si and ^{nat}Si samples could be determined for any of the observed p states. The impurity isotope shift has the sign as predicted for S^+ p states with $E(^{32}S)-E(^{34}S)=+1.41$ cm^{-1} (+0.71 cm^{-1} or +87.4 μeV per amu) This confirms a previously published result for the $2p_\pm$ transition[16] and clarifies that positive and negative S and Se isotope shifts can be observed for different absorption transitions. Our Se diffused samples did not have strong enough absorption for the study of transitions other than $^{77}Se^+$ $2p_\pm$, thus we cannot improve on the Se^+ p-state data which has been previously reported.[8]

It should also be noted that the three S^+ $2p_\pm$ lines in ^{nat}Si and ^{28}Si shown in Fig. 5 appear to have some unresolved structure on the high-energy side. We also observe this for the $^{77}Se^+$ $2p_\pm$ transition shown in the same figure, where the splitting is clearly resolved. While the splitting is reproducible in several samples that are otherwise of excellent quality, the origin of this fine structure remains unclear. A summary of the different isotope dependent energies for the $2p_\pm$ transitions of S^+ and Se^+ is given in Table III.

TABLE III. Energies and FWHM (in cm^{-1}) of the S^+ and Se^+ $2p_\pm$ transition with different host and impurity isotopic compositions.

$2p_\pm$	Energy	FWHM
^{nat}Si:^{32}S	4742.687	2.02
^{28}Si:^{32}S	4742.499	2.16
^{30}Si:^{32}S	4745.296	2.37
^{nat}Si:^{34}S	4741.276	2.29
^{28}Si:^{77}Se (I)	4577.598	1.05
^{28}Si:^{77}Se (II)	4578.932	0.86

B. Se^+ hyperfine splitting

^{77}Se has a nuclear spin of $I=1/2$ and thus Se^+ has a hyperfine splitting in the ground state as shown in Fig. 6. The $^{77}Se^+$ $1s(T_2)$ Γ_7 hyperfine components are separated by 0.056 cm^{-1}. This is in excellent agreement with the $^{77}Se^+$ ground-state hyperfine splitting determined by magnetic resonance.[19] When a magnetic field is applied, the electronic and nuclear spin contributions can be separated. At suffi-

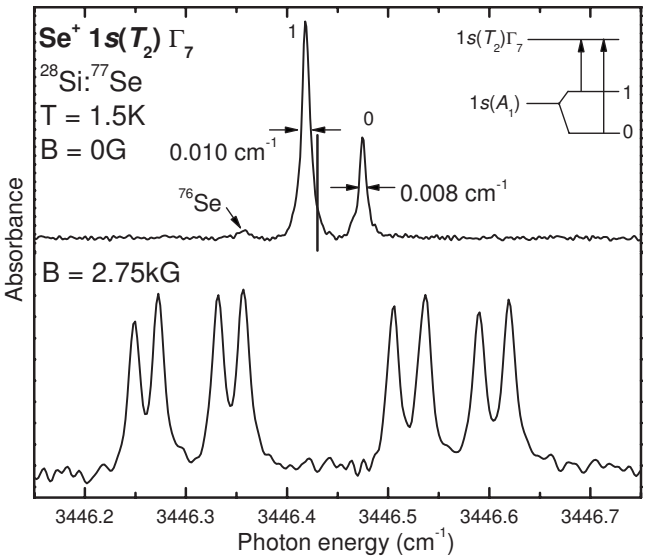

FIG. 6. Spectrum of the $^{77}Se^+$ $1s(T_2)$ Γ_7 transition in ^{28}Si. Top: without external magnetic field showing the ground-state hyperfine splitting. The absorption lines are extremely narrow, with the singlet having a FWHM of only 0.008 cm^{-1} at a spectral resolution of 0.005 cm^{-1}. The vertical line is half way between the ^{76}Se and ^{78}Se energies. Bottom: with an external magnetic field of 2.75 kG. The doublet splits into eight transition lines according to the level diagram in Fig. 7. Spectrum recorded with a resolution of 0.01 cm^{-1} both taken at 1.5 K.

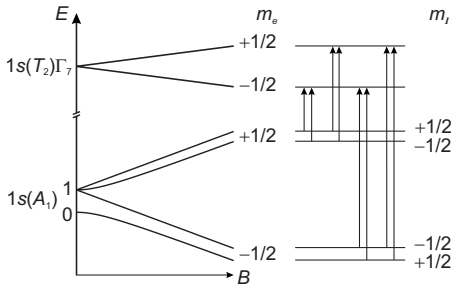

FIG. 7. A level diagram for the Se^+ $1s(T_2)$ Γ_7 Zeeman transitions indicating the origin of the components shown in Fig. 6. $1s(A_1)$ is the Se^+ ground state, and m_e and m_I are the electronic and nuclear spins, respectively. The indicated transitions are in order of increasing energy from left to right.

ciently high fields the hyperfine doublet transforms into eight peaks as can be seen in Fig. 6. The level diagram in Fig. 7 shows the hyperfine splitting of the ground state and the splitting due to the electron spin of the excited $1s(T_2)$ Γ_7 state with and without external magnetic field. The arrows indicating the possible transitions are in order of increasing energy and explain the origin of the four groups of two peaks each that are observed in the spectrum (Fig. 6). The fan diagram in Fig. 8 summarizes the behavior of the Se^+ $1s(T_2)$ transition vs magnetic field. The electron Zeeman splitting of the ground state shows a g factor of 2.0057, in agreement with magnetic resonance experiments,[19] while the excited state shows a splitting with a g factor of 0.644. These figures demonstrate that under an applied magnetic field the electronic and nuclear spins of $^{77}Se^+$ can be determined by an optical measurement.

C. S^0 and Se^0 centers

The S^0 $1s(T_2)$ transition is shown in Fig. 9 for different host and impurity isotopic compositions. The spectra show

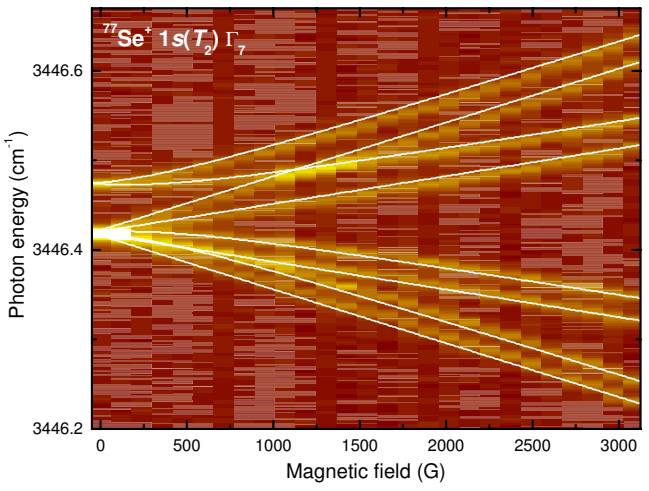

FIG. 8. (Color online) The Zeeman splittings of the $^{77}Se^+$ $1s(T_2)$ Γ_7 transition in ^{28}Si are shown as a fan diagram, where the color/gray scale corresponds to the magnitude of the absorbance, where brighter shades stand for stronger absorbance. The overlaid lines are a fit with g factors of 2.0057 for the ground state and 0.644 for the excited state.

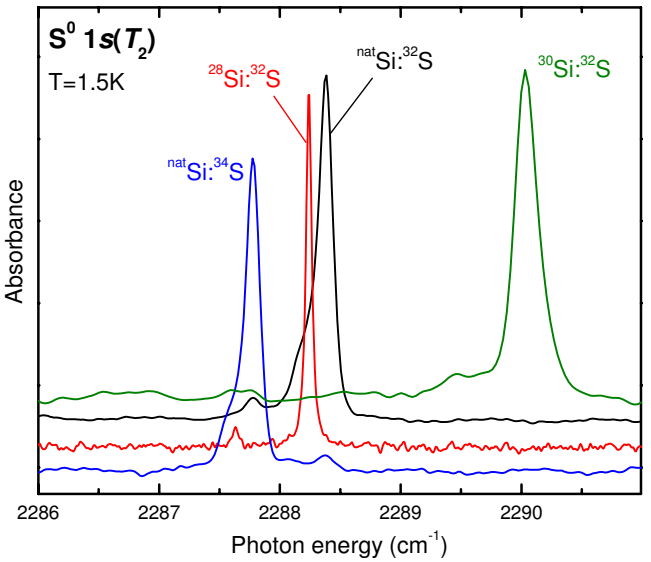

FIG. 9. (Color online) S^0 $1s(T_2)$ in four different samples. Host (Si) and impurity (S) isotope shift are present. All spectra were recorded at a temperature of 1.5 K with resolutions of less than 0.100 cm^{-1} (0.020 cm^{-1} for ^{28}Si).

the Si host isotope shift as well as the S impurity isotope shift $[E(^{32}S)-E(^{34}S)=+0.61\ cm^{-1}$, that is $+0.31\ cm^{-1}$ or $+37.8\ \mu eV$ per amu]. The noticeable shoulders in ^{nat}Si and ^{30}Si suggest that the absorption lines might have unresolved satellites due to LVMs involving Si nearest neighbors similar to those discussed for S^+ $1s(T_2)$. We observe significantly narrower linewidths in ^{28}Si. The absorption line of $^{34}S^0$ $1s(T_2)$ in $^{28}Si:^{34}S$ is 100% Lorentzian and has a FWHM of 0.024 cm^{-1}, reflecting that the width is dominated by homogeneous lifetime broadening.

Figure 10 shows the Se^0 $1s(T_2)$ transition in three differ-

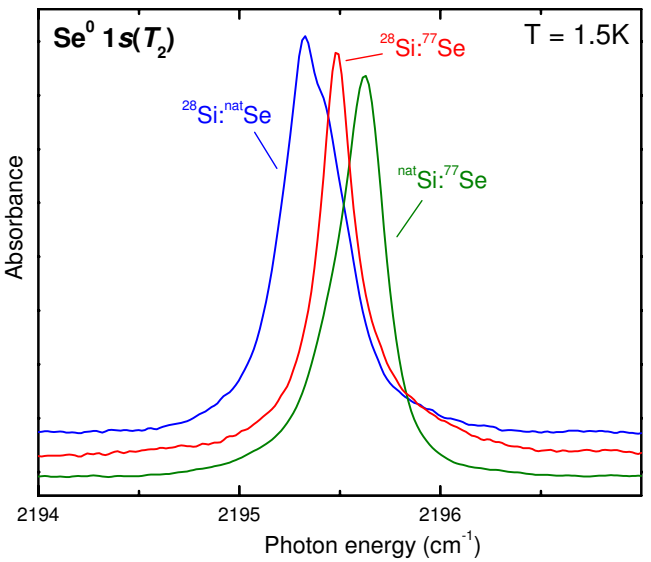

FIG. 10. (Color online) Se^0 $1s(T_2)$ in three different samples. Host (Si) and impurity (Se) isotope shift are present with the ^{nat}Se peak shifted to lower energy than ^{77}Se. All spectra were recorded at a temperature of 1.5 K with a resolution of 0.05 cm^{-1}.

TABLE IV. Energies and FWHM (in cm^{-1}) of S^0 and Se^0 $1s(T_2)$ in samples of different host and impurity isotopic composition.

$1s(T_2)$	^{34}S	^{32}S	^{nat}Se	^{77}Se
^{28}Si	2287.631	2288.240	2195.328	2195.491
FWHM	0.024	0.047	0.36	0.24
^{nat}Si	2287.774	2288.385		2195.599
FWHM	0.14	0.21		0.30
^{30}Si		2290.041		
FWHM		0.23		

ent samples. The $^{28}Si:^{77}Se$ sample exhibits a symmetric line shape. The $^{28}Si:^{nat}Se$ sample shows that for this transition such as for all other transitions except Se^+ and S^+ $1s(T_2)$ the heavier isotopes have a smaller binding energy. Even though the separate isotopes are not resolved in $^{28}Si:^{nat}Se$ it is clear that the peak is shifted to lower energy due to the high natural abundance of ^{80}Se of 49.6%. The peak of $^{nat}Si:^{77}Se$ is shifted to higher energy. The ^{77}Se samples show a near 100% Lorentzian line shape even in ^{nat}Si. Their FWHM is thus lifetime limited. Table IV gives a summary of the energies and FWHM of S^0 and Se^0 $1s(T_2)$ transitions in different samples.

Much has been reported about S^0 p states in the past. The S concentration of our ^{nat}Si sample is relatively low. Due to the reduced concentration broadening we see two more highly excited states than shown in previously published results for S^0.[7–9,20] Those transitions are $7f_{\pm}(2561.47\ cm^{-1})$ and $7h_{\pm}(2562.06\ cm^{-1})$, where labels were assigned with the help of published data given for S^0 and S_2^0.[8,9] Absorption transitions up to $6p_{\pm}$ can be observed in the ^{28}Si sample. The S isotope shift between the samples doped with ^{32}S and ^{34}S is $E(^{32}S)-E(^{34}S)=(+0.65\pm0.02)\ cm^{-1}$ $(+0.33\ cm^{-1}$ or $+40.3\ \mu eV$ per amu). As expected it is constant for all transitions. Some of our peaks in ^{nat}Si and ^{30}Si show relatively strong asymmetries that can contribute to a minor shift in the determined peak energy. However, this peak shape has been observed before for B and P absorption lines in Si,[4] leading to the conclusion that it is an unresolved Si nearest-neighbor isotope effect. We did not work toward improving on existing data[8] for Se^0 p states.

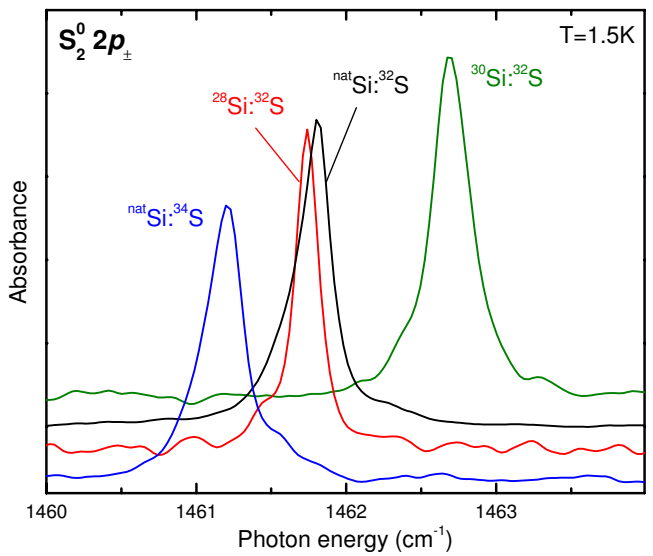

FIG. 11. (Color online) S_2^0 $2p_{\pm}$ in four different samples. Both, the host (Si) and impurity (S) isotope shift are present. All spectra were recorded at a temperature of 1.5 K with a resolution of $0.100\ cm^{-1}$.

TABLE V. Energies and FWHM (in cm^{-1}) of the S_2^0 $2p_{\pm}$ absorption line in samples of different host and impurity isotopic composition.

S_2^0 $2p_{\pm}$	^{34}S	^{32}S
$^{28}Si:^{nat}S$	1460.98	1461.736
FWHM		0.180
$^{nat}Si:^{nat}S$	1461.211	1461.809
FWHM	0.30	0.28
$^{30}Si:^{nat}S$		1462.697
FWHM		0.30

D. S_2^0 and Se_2^+ centers

Our samples were prepared in a way to keep the amount of S_2 and Se_2 pair formation at a minimum. Hence we generally do not observe strong absorption lines due to such pairs. Nevertheless the S_2^0 $2p_{\pm}$ transition was strong enough in all samples to obtain values for position and width of the absorption line (Table V). Figure 11 shows the S_2^0 $2p_{\pm}$ absorption lines in our samples. It is apparent that the host isotope enrichment has only a small influence on the linewidth, which is limited by lifetime broadening. For Se only the $1s(E^-)(2146.32\ cm^{-1})$ and $1s(A^-)(2398.78\ cm^{-1})$ of $^{77}Se_2^+$ in ^{28}Si could be observed

V. CONCLUSION

These results show that the use of highly enriched ^{28}Si eliminates the inhomogeneous isotope broadening inherent to ^{nat}Si. As seen for shallow impurities, this dramatically improves some aspects of the spectroscopy of well-known deep defects and impurity centers. In the case of sulfur we present results regarding isotope effects in enriched ^{28}Si and ^{30}Si. We can identify satellite peaks at the S^+ $1s(T_2)$ transition and observe the impurity isotope dependent energy shift, verifying previous observations.[7,16] For the Se double donor we have been able to resolve the hyperfine splitting in the $^{77}Se^+$ $1s(T_2)$ Γ_7 transition. This allows for the optical detection of both, the electronic and nuclear spins. The S and Se samples also exhibit an energy shift depending on the host isotope enrichment. The S^+ and $^{77}Se^+$ $1s(T_2)$ Γ_7 transitions are, with their FWHM of only $0.008\ cm^{-1}$, the sharpest impurity electronic absorption transition ever observed in a semiconductor. In the case of Se this narrow linewidth, together with the resolved hyperfine splitting, may have applications in quantum computing. Nuclear spins of chalcogen impurities have already been suggested for use as qubits.[21]

ACKNOWLEDGMENTS

This work was supported by NSERC and A.Y. thanks NSERC for additional support. We thank B. Pajot for allowing us to use his $^{nat}Si:^{nat}Se$ spectrum and for useful discussions.

*thewalt@sfu.ca

[1] D. Karaiskaj, J. A. H. Stotz, T. Meyer, M. L. W. Thewalt, and M. Cardona, Phys. Rev. Lett. **90**, 186402 (2003).
[2] D. Karaiskaj, T. A. Meyer, M. L. W. Thewalt, and M. Cardona, Phys. Rev. B **68**, 121201(R) (2003).
[3] M. L. W. Thewalt, Solid State Commun. **133**, 715 (2005).
[4] M. Steger, A. Yang, D. Karaiskaj, M. L. W. Thewalt, E. E. Haller, J. W. Ager III, M. Cardona, H. Riemann, N. V. Abrosimov, A. V. Gusev, A. D. Bulanov, A. K. Kaliteevskii, O. N. Godisov, P. Becker, and H.-J. Pohl, Phys. Rev. B **79**, 205210 (2009).
[5] M. L. W. Thewalt, M. Steger, A. Yang, M. Cardona, H. Riemann, N. V. Abrosimov, M. F. Churbanov, A. V. Gusev, A. D. Bulanov, I. D. Kovalev *et al.*, Physica B **401-402**, 587 (2007).
[6] M. Steger, A. Yang, M. L. W. Thewalt, M. Cardona, H. Riemann, N. V. Abrosimov, M. F. Churbanov, A. V. Gusev, A. D. Bulanov, I. D. Kovalev *et al.*, Physica B **401-402**, 600 (2007).
[7] B. Pajot, B. Clerjaud, and M. D. McCluskey, Phys. Rev. B **69**, 085210 (2004).
[8] E. Janzen, R. Stedman, G. Grossmann, and H. G. Grimmeiss, Phys. Rev. B **29**, 1907 (1984).
[9] B. Pajot, G. Grossmann, M. Astier, and C. Naud, Solid State Commun. **54**, 57 (1985).
[10] H. G. Grimmeiss, E. Janzen, and K. Larsson, Phys. Rev. B **25**, 2627 (1982).
[11] P. J. Dean, R. A. Faulkner, and S. Kimura, Phys. Rev. B **2**, 4062 (1970).
[12] A. Yang, M. Steger, D. Karaiskaj, M. L. W. Thewalt, M. Cardona, K. M. Itoh, H. Riemann, N. V. Abrosimov, M. F. Churbanov, A. V. Gusev, *et al.*, Phys. Rev. Lett. **97**, 227401 (2006).
[13] M. L. W. Thewalt, A. Yang, M. Steger, D. Karaiskaj, M. Cardona, H. Riemann, N. V. Abrosimov, A. V. Gusev, A. D. Bulanov, I. D. Kovalev *et al.*, J. Appl. Phys. **101**, 081724 (2007).
[14] M. Steger, A. Yang, N. Stavrias, M. L. W. Thewalt, H. Riemann, N. V. Abrosimov, M. F. Churbanov, A. V. Gusev, A. D. Bulanov, I. D. Kovalev *et al.*, Phys. Rev. Lett. **100**, 177402 (2008).
[15] J. W. Ager III, J. W. Beeman, W. L. Hansen, E. E. Haller, I. D. Sharp, C. Liao, A. Yang, M. L. W. Thewalt, and H. Riemann, J. Electrochem. Soc. **152**, G448 (2005).
[16] R. A. Forman, Appl. Phys. Lett. **37**, 776 (1980).
[17] V. Heine and C. H. Henry, Phys. Rev. B **11**, 3795 (1975).
[18] S. M. Kogan, Sov. Phys. Semicond. **13**, 1131 (1979).
[19] H. G. Grimmeiss, E. Janzén, H. Ennen, O. Schirmer, J. Schneider, R. Wörner, C. Holm, E. Sirtl, and P. Wagner, Phys. Rev. B **24**, 4571 (1981).
[20] W. E. Krag, W. H. Kleiner, and H. J. Zeiger, Phys. Rev. B **33**, 8304 (1986).
[21] G. P. Berman, G. D. Doolen, P. C. Hammel, and V. I. Tsifrinovich, Phys. Rev. Lett. **86**, 2894 (2001).